Title of proposed research:
Efficient Design Tool for 2D and 3D NIMs Photonic Crystals (AOARD-07-4024)

Key researchers: Professor Joshua Le-Wei Li

Affiliation: National University of Singapore

Address: Dept of Electrical & Computer Engineering

Tel:, Fax:, email: 65-6516-6658; 65-6779-1103; LWLi@nus.edu.sg

Past AOARD or US government support: AOARD-064031.

Table of content

1. Abstract

For the past many years, the design of the photonic crystals of complicated 3-D structures was usually made by suing the finite-difference time-domain (FD-TD) method. The method is very slow when an electrically large-scaled problem is characterized. Also, quite often, the problem is considered in the frequency domain for a spectrum of the light waves. Although the other methods (see more details in the later text) are also applicable, but they are either less efficient in speed and accuracy, or applicable to time domain. The frequency domain work will have to require the Fourier transform and additional time and efforts are required.

This proposal will explore applying the volume integral equations for characterizing and designing the 2D and even 3D structured photonic crystals. Because of many different choices of the basis functions for the volume cells, the approach will be very flexible in handling many different types of photonic crystals of various geometrical structures. Most importantly, the proposed approach can be accelerated by the fast solver so that many theoretical untouchable large scaled problems to become solve-able and previously slow converged problems to be fast in convergence and accurate in solution.

2. Introduction

Band structures are essential characteristics of photonic crystals (PCs), from which possible photonic band gaps (PBGs) can be identified [1-3]. For frequencies within the PBGs, wave propagation is forbidden and many photonic devices have been proposed and designed based on such phenomenon. In particular, twodimensional (2-D) PCs composed of either dielectric rods or air columns have been widely employed in many applications such as waveguiding, resonant cavity formation, and wavelength _ltering. In this paper, we propose a novel analysis scheme with excellent numerical convergence behavior and accuracy for

Report Documentation Page

Form Approved
OMB No. 0704-0188

1. REPORT DATE	2. REPORT TYPE	3. DATES COVERED
28 JAN 2008	**FInal**	**22-02-2007 to 22-03-2008**

4. TITLE AND SUBTITLE
Efficient Design Tool for 2D and 3D NIMS Photonic Crystals

5a. CONTRACT NUMBER
FA48690714024

5b. GRANT NUMBER

5c. PROGRAM ELEMENT NUMBER

6. AUTHOR(S)
Joshua Li Wei Li

5d. PROJECT NUMBER

5e. TASK NUMBER

5f. WORK UNIT NUMBER

7. PERFORMING ORGANIZATION NAME(S) AND ADDRESS(ES)
National University of Singapore,10 Kent Ridge Crescent,Singapore 119260,Singapore,sp,119260

8. PERFORMING ORGANIZATION REPORT NUMBER
N/A

9. SPONSORING/MONITORING AGENCY NAME(S) AND ADDRESS(ES)
AOARD, UNIT 45002, APO, AP, 96337-5002

10. SPONSOR/MONITOR'S ACRONYM(S)
AOARD

11. SPONSOR/MONITOR'S REPORT NUMBER(S)
AOARD-074024

12. DISTRIBUTION/AVAILABILITY STATEMENT
Approved for public release; distribution unlimited

13. SUPPLEMENTARY NOTES

14. ABSTRACT

For the past many years, the design of the photonic crystals of complicated 3-D structures was usually made by suing the finite-difference time-domain (FD-TD) method. The method is very slow when an electrically large-scaled problem is characterized. Also, quite often, the problem is considered in the frequency domain for a spectrum of the light waves. Although the other methods (see more details in the later text) are also applicable, but they are either less efficient in speed and accuracy, or applicable to time domain. The frequency domain work will have to require the Fourier transform and additional time and efforts are required. This work explores applying the volume integral equations for characterizing and designing the 2D and even 3D structured photonic crystals. Because of many different choices of the basis functions for the volume cells, the approach will be very flexible in handling many different types of photonic crystals of various geometrical structures. Most importantly, the proposed approach can be accelerated by the fast solver so that many theoretical untouchable large scaled problems to become solve-able and previously slow converged problems to be fast in convergence and accurate in solution.

15. SUBJECT TERMS
Optics, Computational Electromagnetics, Photonic Crystals

16. SECURITY CLASSIFICATION OF:			17. LIMITATION OF ABSTRACT	18. NUMBER OF PAGES	19a. NAME OF RESPONSIBLE PERSON
a. REPORT	b. ABSTRACT	c. THIS PAGE			
unclassified	**unclassified**	**unclassified**	**Same as Report (SAR)**	**17**	

calculating the band structures of 2-D PCs. The currently most used numerical methods for such calculation have been the planewave expansion (PWE) method [3-6] and the finite-difference time-domain (FDTD) method [7,8]. The finite difference eigenvalue problem formulation has also been employed by Yang [9] and Shen et al. [10], and more recently by Yu and Chang [11] based on the Yee mesh as often employed in the FDTD method [12]. The Yee-mesh-based formulation was named as the finite difference frequency-domain (FDFD) method. Yu and Chang [11] used the FDFD method to analyze the band structures of 2-D PCs with either square or triangular lattice and adopted a fourth-order accurate compact finite difference scheme [13] to increase numerical efficiency and accuracy. Although the FDFD method offers results with accuracy comparable to those obtained using the MIT Photonic-Bands (MPB) package [14] based on the PWE method, the numerical convergent speed was found not to be uniformly fast among different bands in both methods.

References

[1] E. Yablonovitch, Phys. Rev. Lett. 58, 2059 (1987).
[2] S. John, Phys. Rev. Lett. 58, 2486 (1987).
[3] J. D. Joannopoulos, R. D. Meade, and J. N. Winn, Photonic Crystal: Modeling the Flow of Light (Princeton University Press, Princeton, NJ, 1995).
[4] K. M. Ho, C. T. Chan, and C. M. Soukoulis, Phys. Rev. Lett. 65, 3152 (1990).
[5] R. D. Meade, K. D. Brommer, A. M. Rappe, and J. D. Joannopoulous, Appl. Phys. Lett. 61, 495 (1992).
[6] M. Plihal and A. A. Maradudin, Phys. Rev. B 44, 8565 (1991).
[7] C. T. Chan, Q. L. Yu, and K. M. Ho, Phys. Rev. B 51, 16635 (1995).
[8] M. Qiu, and S. He, Appl. Phys. 87, 8268 (1992).
[9] H. Y. D. Yang, IEEE. Trans. Microwave Theory Tech. 34, 2688 (1996).
[10] L. Shen, S. He, and A. Xiao, Comp. Phys. Commun. 143, 213 (2002).
[11] C. P. Yu and H. C. Chang, Opt. Express 12, 1397 (2004).
[12] K. S. Yee, IEEE Trans. Antennas Propagat. AP-14, 302 (1966).
[13] A. Yefet and E. Turkel, Appl. Numer. Math. 33, 125 (2000).
[14] S. G. Johnson and J. D. Joannopoulos, Opt. Express 8, 173 (2001).

The *scientific* objective is to develop an efficient tool for designing and characterizing NIMs photonic crystals. The Singapore team (Nat'l Univ of S'pore) will work together with the US Team (Univ of Colorado, at Boulder) to make the the following suggested structures by US side:

- Si-based 2D photonic crystal structures (hexagonal array of holes): thickness = 300nm, hole dimater =340nm, lattice consntant = 540nm;
- Si-polymer flexible 2D photonic crystal structures (hexagonal array of Si rods in polymer): thickness = 390nm, rod dimater =340nm, lattice consntant = 615nm.

For the 2D structures in (1) and (2), Dr Park's group has used thicknesses as thin as 200nm but never went above 390nm. Hole (or rod) diameters and lattice constants are of course variable. They target near-infrared operation around 1.5 um. As found in references, Dr Park used the devices with the exact parameters given above. In these 2D devices, Dr Park is primarily interested in looking into the out-of-plane scattering problems which critically affect the losses in our system. Therefore, the Spore team will work hard to come up with an efficient tool for the US side to use for designs and characterizations.

Also in the future, the following configurations will be considered in the designs:

- Gold nanoshell 3D photonic crystal: core (silica) diameter = 418nm, gold shell thickness = 20nm (optionally additional silica coating of 10-20nm). For the 3D structures in (3), we can make spheres/shells whose diameters range from 100 - 500nm. Gold shell thickness is fairly constant at 20nm.

We are interested in obtaining 3D photonic band structures using the exact gold dielectric constant and possible plasmon resonances in these highly modulated structures.

But this will not be put in the scope of the present research proposal, because of the time restriction. Code development really needs time and the debugging sometimes can be very time consuming.

3. Approach

To make a design of the NIMs photonic crystals, the following approaches are proposed:

- Starting from the Maxwell equations (for the sizes less than several nano meters, the Maxwell's equations are still considered to be more accurate than the quantum mechanic theory);
- Volume integral equations will be used to discretize the structures of the photonic crystals, where various shaped periodic structures will be identified and characterized;
- The vector basis functions will be chosen as "the volume Schaubert–Wilton–Glisson (SWG) basis functions";
- Nano-scaled NIMs homogeneous materials are considered in the design and characterizations
- Photonic band gap structures will be properly designed so as to exhibit the negative refraction and also to have improved imaging properties.

Also, this project will integrate with the fast solver by implementing the algorithms and codes into the design procedure. Among the fast solvers, the adaptive integral equation (AIM) method, and pre-corrected fast Fourier transform method (pFFT) will be specifically considered. The AIM and pFFT use the same ideal and procedure but different mapping techniques to solve the problem for the design. Therefore, we will opt the pFFT as the algorithm for the fast solver development. The PI has invested US$650,000 on the fast algorithms design and the method adopted for the proposed project is very promising and efficient.

4. Pay-off

- From the research advances or accomplishment, it is then possible to make the 2D and 3D photonic crystal designs in a fast and efficient way which the current methodologies are restricted or impossible to be utilized or extended to apply.
- The commercial packages are far slower to produce the reasonably good or satisfactory results. In this sense, the advances could not only make the practical designs of the NIMs photonic crystals of good performance possible, fast and efficient, but also push the computational science or physics or the numerical techniques applied to electromagnetics to a next height.

5. Summary

- UNIQUENESS: Again, it is indicated that the proposed project will implement the fast algorithms for the metamaterial designs. This will push the existing numerical technologies for the metamaterial designs into the next height. Also, this is a unique approach, and it can achieve what the commercial software packages can never accomplish.

- INNOVATION: After the algorithms will be developed, they will be utilized to generate some new designs of the metamaterials which could lead a few new materials into the frontier. Some

metamaterials of new and novel features will be designed and synthesized.

- PAY-OFF: To further develop the existing technology into the next heights, the implementation of the AIM will be made and the new upper limit of software packages used in the metamaterial designs can be expected. With the to-be-developed algorithms, some new and novel features of the metamaterials will be achieved and found.

6. References

Papers related to the metamaterials

[1] Hao-Yuan She, Le-Wei Li, Soo Jin Chua, Wei-Bin Ewe, Olivier J.F. Martin, and Juan R. Mosig, "Enhanced Backscattering by Multiple NanoCylinders Illuminated by TE Plane Wave", Journal of Applied Physics, vol. 104, no. 1, 064310, September 2008

[2] Le-Wei Li, Zhong-Cheng Li, Hao-Yuan She, Said Zouhdi, Juan R. Mosig, and Olivier J.F. Martin, "A New Closed Form Solution to Light Scattering by Spherical Nanoshells", IEEE Transactions on Nanotechnology, vol. 7, 2008

[3] Le-Wei Li and Hao-Yuan She, "High Energy Scattered by Silver Coated Nano Structures", International Journal of Microwave and Optical Technology, vol. 3, no. 3, pp. 150-156, July 2008

[4] Hao-Yuan She, Le-Wei Li, Olivier J.F. Martin, and Juan R. Mosig, " Surface Polaritons of Coated Cylinders Illuminated by Normal-Incident TM and TE Plane Waves", Optics Express, vol. 16, no. 2, pp. 1007-1019, January 2008

[5] Cheng-Wei Qiu, Nawaz Burokur, Said Zouhdi, and Le-Wei Li, " Chiral Nihility Effects on Energy Flow in Chiral Materials", Journal of the Optical Society of America A, vol. 25, no. 1, pp. 55-63, January 2008

[6] CW Qiu, HY Yao, SN Burokur, S Zouhdi, and LW Li, "Electromagnetic Scattering Properties in a Multilayered Metamaterial Cylinder", IEICE Transactions on Electronics, vol. E-90-B, no. 9, September 2007

[7] CW Qiu, HY Yao, LW Li, S Zouhdi, and TS Yeo, "Eigenfunctional Representation of Dyadic Green's Functions in Multilayered Gyrotropic Chiral Media", Journal of Physics A: Mathematical and Theoretical, vol. 40, no. 21, pp. 5751-5766, May 2007

[8] CW Qiu, HY Yao, LW Li, S Zouhdi, and TS Yeo, "Backward waves in magnetoelectrically chiral media: Propagation, impedance, and negative refraction", Physical Review B, vol. 75, no. 15, 155120, 2007

[9] CW Qiu, LW Li, TS Yeo, and S Zouhdi, "Scattering by rotationally symmetric anisotropic spheres: Potential formulation and parametric studies", Physical Review E, vol. 75, no. 2, 026609, January 2007

Papers related to the code development

[1] Xiao Chun Nie, Ning Yuan, Le-Wei Li, and Yeow Beng Gan, "Fast Analysis of RCS over a Frequency Band Using Pre-corrected FFT/AIM and Asymptotic Waveform Evaluation Technique", IEEE Transactions on Antennas and Propagation, vol. 56, no. 11, November 2008

[2] N.V. Venkatarayalu, Yeow-Beng Gan, Robert Lee, and Le-Wei Li, "Application of Hybrid FETD-FDTD Method in the Modeling and Analysis of Antenna", IEEE Transactions on Antennas and Propagation, vol. 56, no. 9, pp. 3068-3072, September 2008

[3] Wei-Bin Ewe, Er-Ping Li, Hong-Son Chu, and Le-Wei Li, "AIM Analysis of Electromagnetic Scattering by Arbitrarily Shaped Magnetodielectric Object", IEEE Transactions on Antennas and Propagation, vol. 55, no. 7, July 2007

[4] Wei-Jiang Zhao, Yeow-Beng Gan, Le-Wei Li, and Chao-Fu Wang, "Effects of an Electrically Large Airborne Radome on Radiation Patterns and Input Impedance of a Dipole Array", IEEE Transactions on Antennas and Propagation, vol. 55, 2007

[5] Wei-Bin Ewe, Le-Wei Li, Che Sau Chang, and Jin-Ping Xu, "AIM Analysis of Scattering and Radiation by Arbitrary Surface-Wire Configurations IEEE Transactions on Antennas and Propagation, vol. 55, no. 1, pp. 162-166, January 2007

[6] Ning Yuan, Tat Soon Yeo, Xiao Chun Nie, Yeow Beng Gan, and Le-Wei Li, "Analysis of Probe-fed Conformal Microstrip Antennas on Finite Ground Plane and Substrate", IEEE Transactions on Antennas and Propagation, vol. 54, no. 2, pp. 554-563, Feb. 2006

[7] Xiao Chun Nie, Ning Yuan, Le-Wei Li, Yeow Beng Gan, and Tat Soon Yeo, "A Fast Combined Field Volume Integral Equation Solution to EM scattering by 3D Dielectric Objects of Arbitrary Permittivity and Permeability", IEEE Transactions on Antennas and Propagation, vol. 54, no. 3, pp. 961-969, March 2006
[8] HY Yao, LW Li, CW Qiu, Q Wu, and ZN Chen, "Scattering Properties of Electromagnetic Waves in a Multilayered Cylinder Filled with Double Negative and Positive Materials", Radio Science, vol. 42, RS2006, RS003509, 2007

7. Resume & representative outputs

PERSONAL DETAILS

Name		
Dr.	Li	Le-Wei @ Joshua
Title	Surname	Given Name

Designation	Organisation	Country of Organisation
Professor	National University of Singapore	Singapore

Postal Address
Dept of Electrical & Computer Engineering National University of Singapore 10 Kent Ridge Crescent, Singapore 119260

Tel	Fax	E-mail
(+65) 6874 6658	(+65) 6779 1103	LWLi@nus.edu.sg

Country of Origin and Nationality			Year of Birth
China	Singapore	N.A.	1961
Country of Origin/Birth	Country of Citizenship	Singapore Permanent Resident? (Yes/No/NA)	

Highest Qualification			
Ph.D.	Monash University, Melbourne	Australia	1992
Type (e.g. Ph.D, D.Phil, M.Sc)	Awarding Institution	Country of Awarding Institution	Year Awarded

Areas of Research (format: area1; area2; etc)
Electromagnetic wave theory Electromagnetic composite materials Wave propagation, scattering and radiation Numerical techniques and fast algorithms Design and analysis of antennas, microwave & RF circuits, and components

8.

9. ACADEMIC, RESEARCH, PROFESSIONAL AND INDUSTRIAL EXPERIENCE

10.

Professional Honours and Awards	
1. IEEE Fellow	2004
2. University Excellent Teacher Award	2004

3.	2003 IEEE AP-S Best Chapter Award (Singapore Chapter), Chapter Chair	2003
4.	China's National Award for Science and Technology Advances (the same level as NSA & NTA in Singapore)	1997
5	Fellow Member of The Electromagnetics Academy, based at MIT	1996
	Honour/Award	Year Awarded

Institutions/Organisations at which you have held an academic/research position (exclude current institution)

1.	Guest Professor	Southeast University, China	2000
2.	Visiting Professor	Tohoku University, Japan	2001
3.	Visiting Professor	Univ of Western Australia	2001
4.	Advisory Professor	CRIRP, China	2002
5.	Visiting Professor	Xidian University, China	2002
6.	Visiting Scientist	MIT, USA	2002
7.	Guest Professor	Harbin Inst of Tech, China	2003
8	Adjunct Professor	Zhejiang University	2005
	Institution/Organisation	Appointment	Period of appointment

Institutions/Organisations with which you have or have had joint research projects in the last five years

1.	Singapore-MIT Alliance, High Performance Computation for Engineered Systems	Fellow
2.	Institute of Communications Research	Faculty Associate
3.	Institute of High Performance Computing	Faculty Associate
4.	Data Storage Institute	Faculty Associate
5.		
	Institution/Organisation	Period of project

Selected publications (list full references of up to 6 publications, and indicate which ones are relevant to this application)

1. LW Li, XK Kang, and MSLeong, *Spheroidal Wave Functions in Electromagnetic Theory*, Wiley: New York, InterScience Series, Nov., 2001
2. LW Li, WY Yin, MS Leong, *Electromagnetic Theory of Complex Media*, Wiley: New York, InterScience Series, December, 2005
3. Hai-Ying Yao, Le-Wei Li, Qun Wu, and Jin Au Kong , "Macroscopic Performance Analysis of Metamaterials Synthesized from Microscopic 2-D Isotropic Cross Split-Ring Resonator Array", *Progress In Electromagnetics Research*, vol. 51, pp. 197-217, in press, 2005
4. Hai-Ying Yao, Wei Xu, Le-Wei Li, Qun Wu, and Tat-Soon Yeo, "Propagation Property Analysis of Metamaterial Constructed by Conductive SRRs and Wires Using the MGS-based Algorithm," IEEE Transactions on Microwave Theory and Techniques *(Special Issue on Metamaterials)*, vol. 53, no. 4, 2005.
5. Wei Xu, Le-Wei Li, and Qun Wu, "Design of Left-Handed Materials with Broad Bandwidth and Low Loss Using Double Resonant Frequency Structure", submitted to *Physical Review E*, 2005

6. Le-Wei Li, Wei Xu, Hai-Ying Yao, Qun Wu, and Tat-Soon Yeo, "Analysis of Novel Metamaterial Synthesized from Mixture of Transmission Line and SRR Using TLM, Submitted to *Physical Review B*	
Some other related papers are attached.	
Research Mentoring	
54 No. of postgradate research students supervised (to date)	**11** No. of postdoctoral students supervised (to date)

Some New Results:

Simulation and Modelling Part: Fast Solver Development for Photonic Crystals

Simulation and modeling of photonic crystals are considered in the project using the fast solver or algorithum. Before the new design results are made, the codes were validated and their accuracy and efficiency are verified. In the testing, if refractive index of the rods n = 3.4, and their diameter d = 0.36a, the corresponding 2-D photonic crystal has a gap from frequency $\omega = \frac{0.302 \times 2\pi c}{a}$ to $\omega = \frac{0.443 \times 2\pi c}{a}$ [1]. For the photonic crystal waveguide (PCW) formed by removing a row of dielectric rods, the lowest-order guiding mode can be supported in the band from $\omega = \frac{0.312 \times 2\pi c}{a}$ to $\omega = \frac{0.38 \times 2\pi c}{a}$. In our simulation, a 3-D model is constructed by assigning the dielectric rods with a finite length h=10a in the direction. The excitation is induced by a z-polarized plane wave incident on the left side of the waveguide at a frequency of $\omega = \frac{0.37 \times 2\pi c}{a}$.

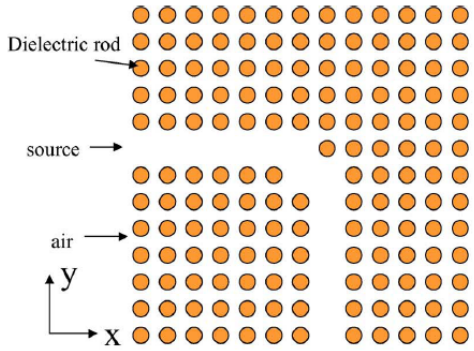

Fig. 1: Photonic crystal based waveguide of finite 3-dimensions.

[1] A. Mekis, J. C. Chen, I. Kurland, S. Fan, P. R. Villeneuve, and J. D. Joannopoulos, "High transmission through sharp bends in photonic crystal waveguides," *Phys. Rev. Lett., vol. 77, pp. 3787–3790, Oct.* 1996.

There are two sets of parameters used in the results:

- ***Case I:*** Si-based 2D photonic crystal structures (hexagonal array of holes): thickness = 300nm, hole diameter =340nm, lattice constant = 540nm; SiO2 is the substrate with thickness = 300nm.
- ***Case II:*** Si-polymer flexible 2D photonic crystal structures (hexagonal array of Si rods in polymer): thickness = 390nm, rod diameter =340nm, lattice constant = 615nm.

The effective index for Si is 3.48, for SiO2 is 1.46, for polyamide is 1.5. I used 11 rows in y direction and 35 rows in x direction. The whole dimension is 36 *a* x 10 *a* x *h*, (*a* is lattice constant and *h* is thickness). The incident wave is a TE plane wave in the *xy* plane, the *k* direction is along y and the *E* direction is along *x*. lambda = 1.5 um.

Si-polymer flexible 2D photonic crystal structures (hexagonal array of Si rods in polymer): thickness = 390 nm, rod diameter = 340 nm, lattice constant = 615 nm. The refractive index of Si is 3.45, and that of polymer is 1.5. The period in *x* direction is 30, in *y* direction is 10. The structure is illuminated by *x*-polarized plane wave in the *y*-direction with wavelength = 1.5 um.

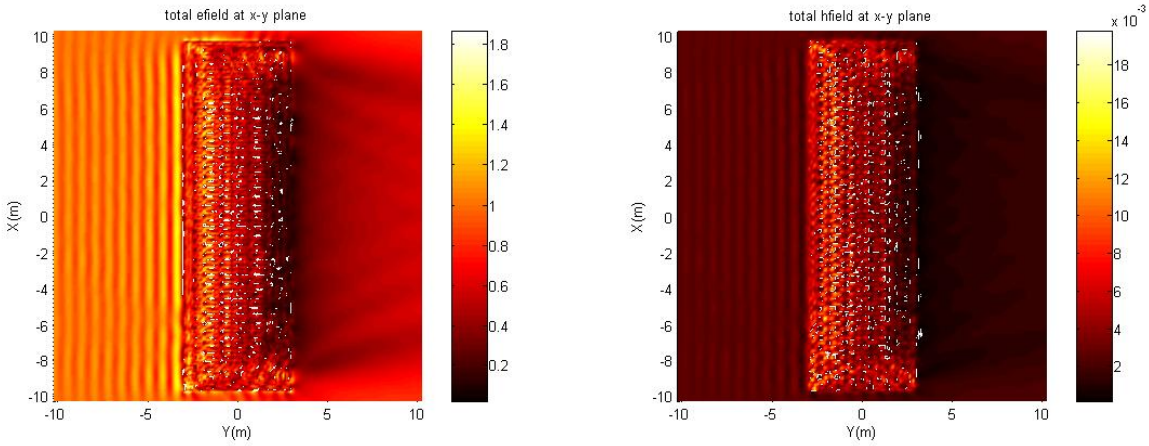

(a) Electric field distribution (b) Magnetic field distribution

Fig. 2: Total electric and magnetic field distributions in the photonic crystal of Case I.

Si-based 2D photonic crystal structures (hexagonal array of air holes): thickness = 300 nm, hole diameter =340 nm, lattice constant = 540 nm; SiO_2 is the substrate with thickness = 300 nm. The refractive index of Si is 3.48, and that of SiO_2 is 1.46. The period in the x-direction is 30, and that in the y-direction is 10. The structure is illuminated by the x-polarized plane wave in the y-direction with a wavelength of1.5 um.

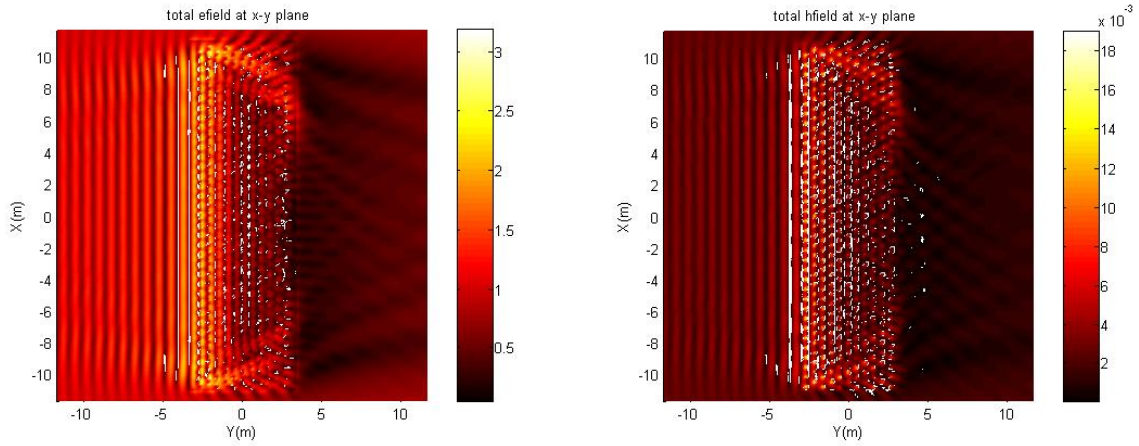

(a) Electric field distribution (b) Magnetic field distribution

Fig. 3: Total electric and magnetic field distributions in the photonic crystal of Case II.

Experiment and Measurement Part: Fabrication and Characterizations of Silicon-Based Photonic Crystal Structures

We report design, fabrication and characterizations of silicon-based photonic crystal structures exhibiting unconventional optical properties such as negative refraction and self-collimation. These devices hold the high promise of enabling novel photonic devices and large-scale integrated optical systems. Experimental demonstrations of the novel optical phenomena reported here are of critical importance because they pave the way to new applications and more sophisticated, fully integrated systems.

The silicon-based photonic crystals were fabricated on silicon-on-insulator (SOI) wafers using the electron-beam lithography and reactive ion etching processes. The photonic crystal patterns were written by the electron beam writing, followed by a lift-off process used to make patterned metallic hard masks on top of the silicon device layer. The pattern was then transferred to the silicon device layer by the anisotropic reactive ion etching process. Optionally, the silicon dioxide lower cladding layer may be etched to create a symmetric, air-suspended structure. Strictly speaking, the modes have fundamental differences between the symmetric, air-suspended structure and the asymmetric structure lying on an oxide layer. The symmetric structure supports clearly defined even/odd modes which possess mirror symmetry with respect to the mirror plane at the center of the photonic crystal layer. For the asymmetric structure, there is no mirror symmetry and therefore the optical modes do not possess any mirror symmetry either. This leads to mode mixing between the even and odd symmetric modes. However, in practice, the index contrast between the silicon device layer and the oxide/air cladding layers is large enough to ignore the relatively small index differences between oxide and air claddings.

For optical characterizations, we incorporate two complementary methods: far-field and near-field measurements. For the far-field measurements, the silicon wafer is mounted vertically and a tunable fiber coupled infrared laser is then butt-coupled to the cleaved edge of the silicon device. Out-of-plane scattered light is collected with an objective lens, sent through the eyepiece lens, and then imaged onto the vidicon infrared camera. For alignment purposes, a visible spectrum lamp illuminates the sample during operation, which is coupled in with a 50/50 beamsplitter. The infrared camera is able to detect both infrared and visible light, although there is substantial chromatic aberration. The far-field characterization setup is schematically shown in Fig. 1(a).

A microscope objective only images light that is scattered from the device or is no longer guided by the silicon device layer, i.e. radiative modes. The evanescent field of a guided wave is invisible to a far-field lens perpendicular to the direction of the waveguide and a near-field technique is needed for accurate detection of evanescent fields. There are other advantages of near-field characterization methods beyond the ability to image otherwise bound modes. One is that very large spatial resolution is possible because evanescent or near-fields carry very high spatial frequency information. We used a near-field scanning optical microscopy (NSOM), which uses a tapered fiber tip coated with a metal to provide large confinement and then scans this over the desired image. The tip is maintained at a very small distance from the surface by monitoring the surface forces in the same manner as an atomic force microscope. Because this surface distance is fractions of a wavelength, resolution higher than the free space diffraction limit is obtained.

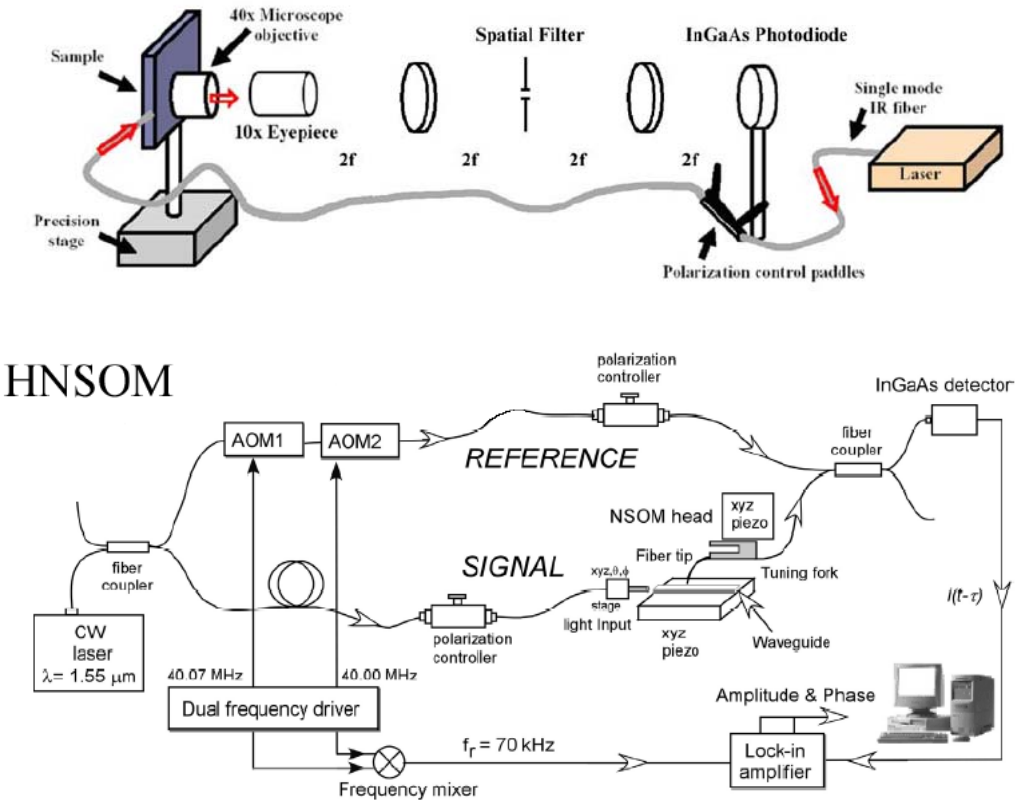

Figure 1. (a) The optical set-up that is capable of measuring quantitative image brightness. The vidicon camera is replaced with a photodetector and a spatial filter or pinhole is used to filter only a certain region of the scattered image. (b) A schematic for heterodyne NSOM. Light from a tunable continuous wave (CW) laser is coupled into two fibers. One port is sent to two acousto-optics modulators (AOM's) where the output is to be used as a reference signal. The other port is sent into the device, via polarization control and an xyz stage. Light is coupled out through the NSOM head, represented as a tuning fork, and then recombined with the reference on the InGaAs detector. The detector is sent to a lock-in amplifier, which is also fed the difference signal that drives the two AOMs. The output phase and amplitude from the lock-in is fed to a computer for post-processing.

Another benefit which is more a result of a scanning microscope than a near-field microscope is that it is possible to do interferometry at each spatial location. Interferometry has two important advantages in this case. The first is that the signal strength can be increased by a couple of orders of magnitude through interferometric heterodyne gain. The signal detected by the scanning probe is very weak, due to both the fast spatial decay of the wave being detected and the low collection efficiency of the subwavelength aperture of the tip. In heterodyne NSOM, the weak signal collected from the tip is coherently mixed with a strong reference signal.

The other large benefit of interferometric NSOM is that both the amplitude and the phase of the bound wave can be observed. In the experimental set-up used in this work, schematically shown in Fig. 1(b), a fiber coupled laser is first sent through an optical amplifier to boost the power up to 100 mW. The laser is then split by a fiber coupler into two arms. The reference arm is sent through two acousto-optic modulators that shift the frequency by 40.07 MHz and then –40 MHz to produce a beam that is detuned by 70 kHz. The other arm is coupled into the PC device. A small portion of this signal is coupled out through the tapered

tip and then both signals are mixed together on a photodetector and then the signal is sent to a lock-in amplifier. In this way, both the amplitude and phase can be evaluated.

Using the fabrication and characterization techniques described above, we investigated two types of silicon-based photonic crystal (PC) structures: negative index photonic crystals and self-collimating photonic crystals. As an example of novel application of negative index PC, we first present a PC total internal reflection (TIR) prism that can operate at small incident angles or even normal incidence. The device understudy has a PC region with a shape of 120°-30°-30° prism where light enters and exits a ΓM-to-silicon interface and is reflected from a ΓK-to-air interface, as shown in Fig. 2(a). Small regions around each 30° vertex have been removed because they do not substantially effect light propagation. Three input waveguides each of which is 3 μm wide and separated from each other by 5 μm, terminate 68 μm from the PC prism, as shown in the lower right of Fig. 2(a). Light couples into a PC mode in the second photonic band where the EFS is flat along the ΓM direction. The beam then propagates with minimal diffraction for 22 μm in the PC, reflects off the ΓK interface and propagates through another 22 μm inside the prism before coupling back out to the silicon slab. The output beam is sampled by a photonic wire array of 1 μm wide wires with center-to-center spacing of 3 μm.

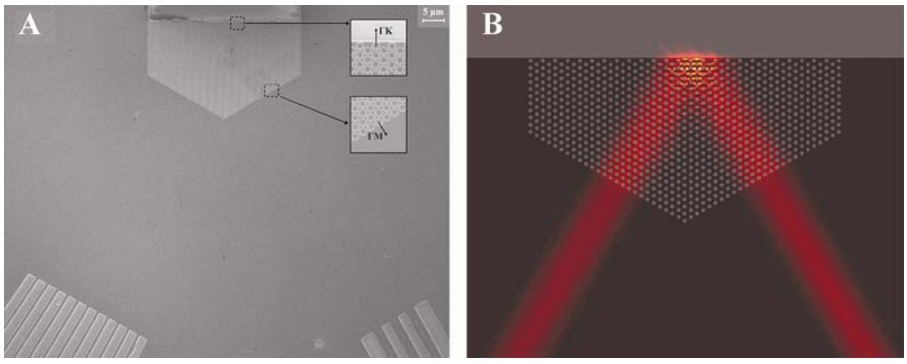

Figure 2. (a) Scanning electron micrograph (SEM) of the fabricated device. The insets show the crystal terminations for the prism input and reflection interfaces. The front half of the prism is surrounded by silicon slab, and behind the prism is an etched out air trench. (b) Numerical simulation of the time averaged square of the E_z (out-of-plane) field. The wave is incident from the bottom right and exits the bottom left. The numerically simulated device is three times smaller than the fabricated device, so diffraction is negligible.

Fig. 2(b) shows a two-dimensional (2D) finite difference time domain (FDTD) simulation of a version of the PC prism that is one-third size of the fabricated sample. The image shows the optical intensity of a TM wave, E field is perpendicular to the substrate, traveling through the device. The PC is composed of 300 nm diameter circular air holes in a hexagonal lattice with a lattice constant of 510 nm in a 300 nm device layer silicon-on-insulator (SOI) platform. At an incident wavelength of 1550 nm, the effective index of the fundamental TM mode in the Si device layer is 2.54. From the FDTD simulation, the magnitude of the reflected wave at the input interface of the prism appears to be very small as seen by the barely visible fringe modulation depth in the input arm. The beam in the PC propagates in the negative refraction regime and forms an internal focus at the reflection edge, and has an external image at the output waveguide array. However, because of the hexagonal distortion that flattens the EFS in the ΓM direction which is typically observed in a triangular PC, diffraction is small and the image plane is difficult to resolve. As the size of the prism increases, diffraction management becomes increasingly more important in order to achieve a large number of resolvable spatial channels in the device and to keep the transverse size of the beam small at the reflection interface.

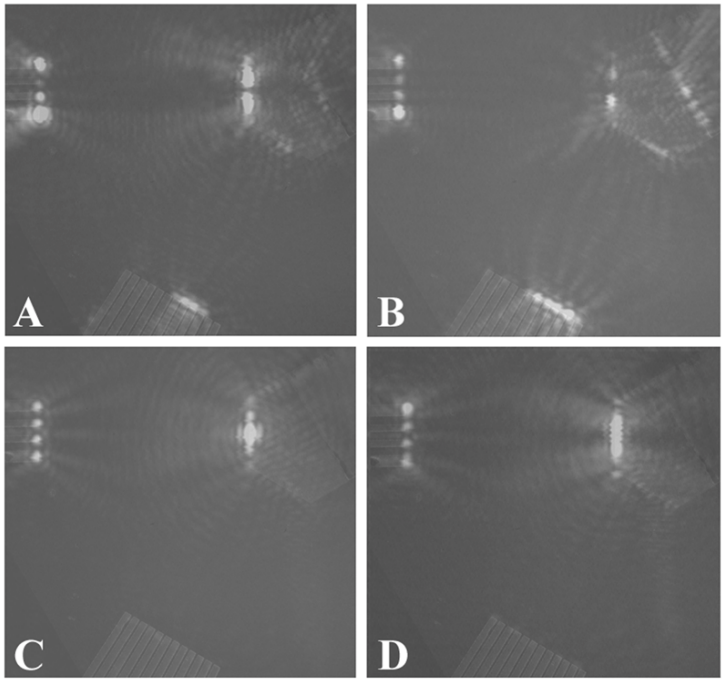

Figure 3. Far-field scattering images of the PC prism. The center input waveguide is illuminated. The scattering images are superimposed on an SEM image to show the device geometry. In each photograph, the input waveguide is at the upper-left, the TIR prism is in the upper-right and the output waveguide array is along the bottom. (a) shows 1542 nm TM polarized illumination, which creates a highly confined output spot that primarily illuminates two output waveguides. (b) shows 1559 nm TM polarized illumination, which has high efficiency and small out-of-plane scattering at each device interface. Scattering from the output waveguide array is significantly brighter than any other region indicating the small losses at the other interfaces. (c) and (d) show 1542 and 1559 nm TE polarized illumination respectively, which does not couple into the PC prism.

Using an objective lens, scattered light from the different interfaces is collected and imaged onto an infrared camera. Far-field scattered light does not give detailed information on the generated evanescent wave or low loss guided regions, but lets us track intensity through the integrated optical system. Scattered intensity is useful for rough estimates on the transmission coefficient of the PC prism and for monitoring the beam width at the output. Fig. 3 shows four far-field images of the device, where Fig. 3(a/c) are with 1542 nm TM/TE illumination, and Fig. 3(b/d) are with 1559 nm TM/TE illumination, respectively. In each figure, the input waveguides are at the top left, where the light is moving from left to right. The guided optical wave is then reflected by the prism where it is finally incident on the output waveguide array located at the bottom of each figure. Fig. 3(a) represents the wavelength which displays the tightest field confinement shown by the small field distribution incident on the output waveguide array. Fig. 3(b) shows the wavelength where reflection losses are the lowest shown by the brightness of the output spot. Although all three terminations of the input waveguides light up, the scattered light does not represent the field in each input waveguide. This scattered light is from the sharp edges of the termination and could be reduced with an inverse taper.

The images in Fig. 3 represent the response when only the middle input waveguide is excited. The field distribution in the 3 μm input guides has a half width at e^{-1} value of 1.19 μm and 1.14 μm for TM and TE respectively. Using a gaussian beam model for propagation, the Rayleigh range (z_o) for the TM mode is

7.44 μm and 8.08 μm for the TE mode. The distance from the termination of the input guide to the start of the output photonic wire array in the folded optical system is 180 μm, which is more than $20z_o$. The wave propagates 68 μm from the input guide to the prism edge, where it diffracts to a full width of 22 μm for TM and 19 μm for TE. The e^{-1} points of the beam just fit into the aperture of the prism, which is 24 μm wide. From Fig. 3(a,c), the TM mode looks slightly larger than the TE mode when it is incident on the prism and is roughly the width of the input interface, which matches the prediction. The beam then propagates through the PC prism in a slow diffraction regime with a small amount of negative curvature, which contracts the beam size. After reflection and propagation through the second silicon slab region, the beam is incident onto the output photonic wire array, where we can measure its transverse size. At the tightest confinement where diffraction is most effectively managed, shown in Fig. 3(a), the beam has a full width of 7-10 μm, which is roughly half the size as it was on the prism entrance and 1/24 of the size it would be if it propagated through 180 μm of uniform silicon slab. The TE mode is effectively filtered out of the system as can be seen from the small amount of light reaching the output in Fig. 3(c,d). The image in Fig. 3(b) shows how efficient the PC prism can be, where the amount of light hitting the output waveguide array is much stronger than the scattered signals at the other interfaces. Numerically, the device is predicted to transmit up to 95% of the light, and though this number is not verified experimentally, the efficiency appears to be high.

Using a heterodyne near-field scanning optical microscope (HNSOM), we measured the amplitude and phase of the guided wave at the reflection interface. Fig. 4(a) and its inset on the right show that the amplitude image of the detected field has a peak at the interface and then exponentially decays into the air trench, while staying at a roughly constant value in the PC. The wavelength of illumination is 1552 nm, which does not give the tightest field confinement at the interface, but gives a strong signal showing a bright evanescent field. The phase of the field in Fig. 4(b) shows that along the reflection interface, the phase varies only in the tangential direction. An evanescent field's momentum vector is real only for the direction parallel to the interface, so the phase should not progress in any other direction. The inset shows a cross-section of the phase 260 nm behind the interface that has a period of 1.42 μm, which is below the free space wavelength, indicating that the wave is evanescent.

The decay constant of the evanescent field is measured to be 1.20 μm, defined as the e^{-1} location of the field amplitude. The inset is obtained by summing a 10 μm wide field along the boundary, and plotting the summation as a function of vertical distance along $\mathbf{Y}$. The summation averages field values over several unit cells of the PC and results in a smooth curve. Field values in the HNSOM image are sampled at an interval of 260 nm, so there are 4-5 measurements in the e^{-1} decay region. A near-field object is convolved with the collection tip, in this case 200 nm. This convolution blurs sharp features by approximately this amount, which increases the measured decay distance. Along the interface, the amplitude is modulated by the surface periodicity of the PC, $\sqrt{3}\boldsymbol{a}$, but this does not describe the phase progression along the TIR interface, as we will see by looking at the tangential phase profile.

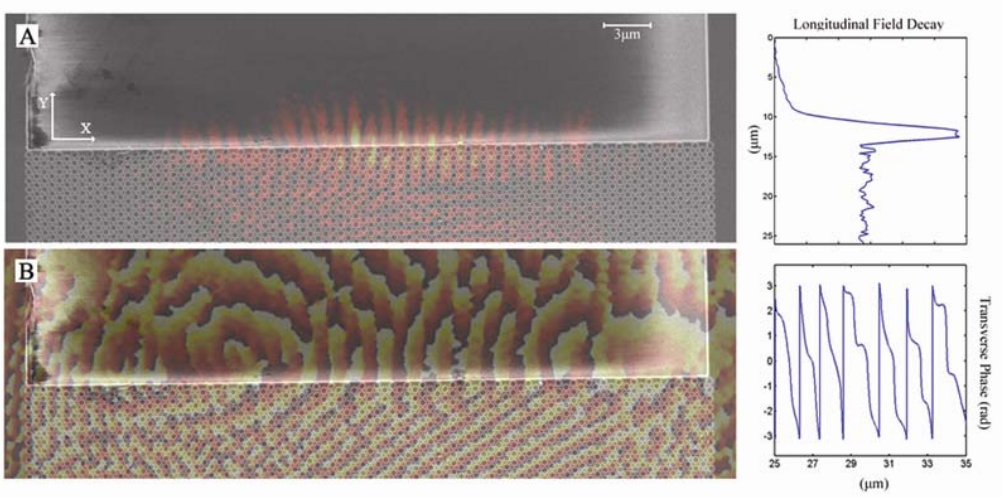

Figure 4. The amplitude and phase images along the reflection interface collected by the HNSOM superimposed on the SEM image to show the geometry. The inset to the amplitude image shows the field amplitude averaged over a 10 μm cross-section plotted vs. **Y**. The inset to the phase image shows the evanescent field phase one sample above the interface in the air region plotted vs. **X**.

The phase image in Fig. 4(b) shows a coherent wave incident into the boundary from the PC and along the interface. The tangential momentum of these two waves is equal according to the boundary condition. By taking a cross-section of the phase image just beyond the interface in the air region, the spatial period of the wave is observed to be 1.42 μm, which gives k_{ev}=1.09k_{air}. The decay constant of an evanescent wave can be predicted from its momentum by the expression $D = 1/\sqrt{k_{ev}^2 - k_{air}^2}$. Using k_{ev}=1.09k_{air}, the decay constant is expected to be 570 nm, which is smaller than the measured value of 1.2 μm. Because the field is spatially confined, there is a spectrum of transverse momentum values at the boundary. Lower spatial frequencies decay slower into the air region, so they have greater influence at large distances from the interface. In order to better understand the spectrum of the evanescent wave, we perform Fourier analysis of the measured complex field. This method also gives insight into the reason for measuring a larger D.

As can be seen in Fig. 5 by the blue curve, the self-collimation regime is located at slightly lower frequency region than negative refraction. For a certain incident spatial bandwidth along the <11> direction, all the excited $\mathbf{k}_{Bloch}$ vectors will be parallel and of the same length, so diffraction will not occur. In order to take advantage of this diffraction free medium, a PC is fabricated in a long narrow strip 10 μms wide and 50 μms long. The PC lattice constant is shrunk from 420 nm in the negative refraction sample to 350 nm because operation in a lower frequency region in the first photonic band is required.

Figure 6(a) shows the geometry of the device. Without the PC in place, a 1.5 μm beam leaves the 2 μm input waveguide and diffracts through the un-patterned slab. The diffraction parameter in the slab is governed by the effective index of the slab mode. After propagation

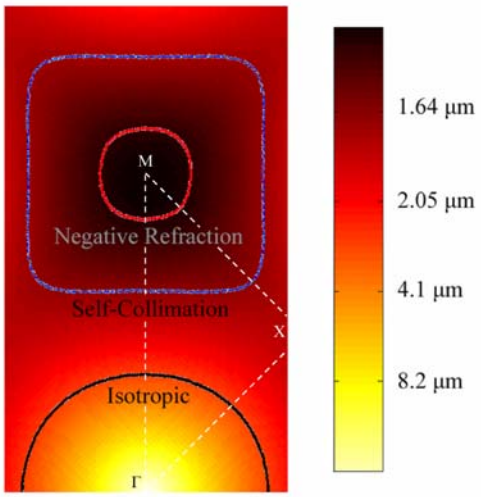

Figure 5. The EFS for the three propagation regimes in the first band. The dispersion diagram is evaluated for a TE-like mode in a square PC with a period of 410 nm and a hole diameter of 295 nm in a 300 nm film of silicon.

through the 50 μm slab region the beam has a width larger than the 10 μm wide output waveguide array, around 16 μm. By comparison, the narrow beam propagating through the PC diffracts only a very small amount, and upon hitting the output waveguide array has a width of 2.25 μms. Similar to the negative refraction experiment, we can analyze the Fourier spectra of the complex field distribution. In this case there is very good agreement with the effective mode index obtained experimentally and the one obtained numerically. Both give an effective index value of 2.23 for the TE polarized self-collimated mode. It is unclear why the accuracy here is so much better than other data, but there were also scans taken with this same sample that also had the previous 15-20% scaling error. The one main difference between the experimental and numerical field data, as can be seen in the phase plot in Fig. 7, is that the numerically calculated field profile looks like it has a much stronger modulation from the geometry of the PC than the experimental data. This strong modulation comes from higher spatial frequency harmonics of the PC lattice that are beyond the resolution of the NSOM.

One interesting feature of a self-collimating material is that it is very robust with respect to the incident field. In a traditional multi-mode waveguide, different modes are excited as a function of the shape of the incident field and its respective overlap with each waveguide mode. These modes then interfere and beat throughout the length of the waveguide, resulting in a noisy and complex light distribution throughout the guide. This noisy field distribution is clearly seen in the multi-mode incident ridge waveguide at the left of Fig. 6b, and 6c. Each of the ridge waveguide modes has some transverse field distribution and regardless of its shape, all of these modes couple into the same PC mode. As can be seen from Fig. 6c, the field distribution inside the PC has a clean intensity distribution with primarily only a single maximum. By inspection of the Fourier spectra of this mode, it is also clear that there is only one effective index for the PC mode, unlike the multi-mode waveguide, where each mode has a distinct effective index. Thus in a self-collimation waveguide, there is no modal dispersion. This is a result of the fact that there is no transverse confinement in a self-collimating waveguide, so there are no discrete index levels.

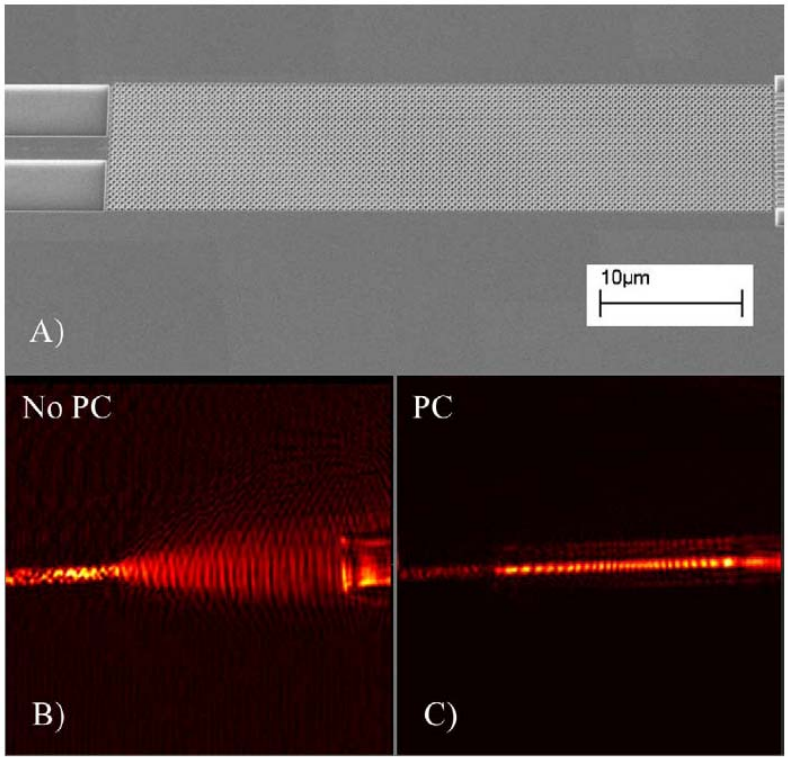

Figure 6. The entire geometry and optical response of the device. (a) shows an SEM with a similar maximum field of view as the NSOM of 70x70 μms in (b) and (c). (b) shows the NSOM without the PC for TE polarization at 1560 nm. (c) shows the same with the PC.

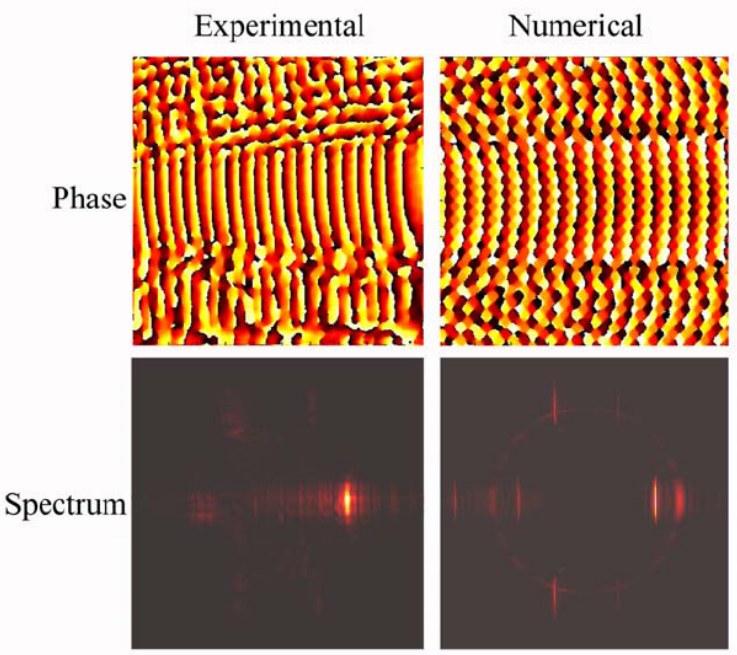

Figure 7. The phase and Fourier spectra of the complex field data collected with the NSOM and through FDTD.

The Fourier spectra of the self-collimating PC show the expected result of a flat EFS. The complex field of the self-collimating mode was taken only inside the PC, so there is not a silicon circle in the spectra like there is in the numerical case where the field of view contained both materials. Many of the same features can be pointed out as in the negative refraction case, i.e. EFS ringing in the propagation direction and the large percentage of energy in the FBZ EFS. Even though there is ringing due to the sharp field of view cut-off, there is clearly only one axial mode of the PC, as predicted.

Another interesting feature of a self-collimating PC waveguide is its spectral dispersion properties. In the first band self-collimation region discussed above, there is non-zero GVD, defined as

$$GVD = \frac{1}{2}\frac{\partial^2 \beta}{\partial \omega^2}$$

where β is the k-vector in the propagation direction. In other words, the self-collimation region in the first band occurs without an inflection point in the band diagram. This is not true for the second band. In the second band, there is an inflection point where the curvature changes sign, and at this location the GVD is zero. In order to compare where the EFS is flat and thus in a self-collimation regime to where there is zero GVD, we can define a parameter for the degree to which an individual k-vector diffracts as

$$D_t = \frac{\partial \omega}{\partial k_t}$$

where k_t is the transverse amplitude of the k-vector. This is done by calculating the entire two-dimensional dispersion surface and taking a numerical derivative in the direction perpendicular to the propagation direction. D_t can be thought of as the group velocity of light perpendicular to the propagation direction,

which should be close to zero for any waveguide. In the second photonic band, the self collimation regime perfectly overlaps the frequency where the GVD=0, thus defining a material where both the diffraction in a certain direction, and the dispersion is zero. These experiments however, have yet to be carried out.

By extracting the PC EFS from the experimental data, we now have quantitative information on both refraction, obtained from the magnitude of k_{Bloch}, and diffraction, obtained by the radius of curvature of k_{Bloch}. This effectively gives us everything we need to characterize the spatial frequency response of the PC. Now that these parameters have been evaluated, more complex designs can be investigated that take advantage of these anomalous refractive and diffractive properties.